Mathematical modeling of metal ion homeostasis and signaling systems

Cui, J.

Publication date
2009

Chapter 3 Detection of A New Calcium Transporter on Yeast Plasma Membrane[8]

3.1 Introduction

As described in Section 1.3.4.1 and Section 1.3.4.2, Ca^{2+} functions as a ubiquitous intracellular messenger by which extracellular factors induce a variety of physiological responses such as proliferation and muscle contraction, etc [5,89]. In budding yeast (*Saccharomyces cerevisiae*), calcium signals are used to effect important adaptations in response to mating pheromones [108], membrane damaging compounds [28], and a variety of environmental stresses such as high salt, high pH, high osmolarity, and others [150].

Due to the sudden increase in extracellular Ca^{2+}, cytosolic free Ca^{2+} level rapidly rises and falls with complex dynamics, as judged by luminescence measurements of yeast cells expressing aequorin [145]. In response to these changes, the universal Ca^{2+} sensor protein calmodulin can bind and activate the protein phosphatase calcineurin, which inhibits the function of Vcx1 and induces the expression of Pmc1 and Pmr1 via activation of the Crz1 transcription factor (see Fig. 3.1a) [50,51,53,111,208]. These calcineurin-sensitive adaptations appear to be crucial for proliferation of yeast cells in high calcium environments. Mathematical modeling of these feedback networks successfully recapitulated the observed changes in aequorin luminescence (see Fig. 2.2c-d). In this chapter, we extend the initial model that was discussed in Chapter 2.

[8] This Chapter is based on: Jiangjun Cui, Jaap Kaandoorp, Olufisayo O. Ositelu, Veronica Beaudry, Alicia Knight, Yves F. Nanfack and Kyle W. Cunningham, Simulating calcium influx and free calcium concentrations in yeast, *Cell Calcium*, in press, (2008).

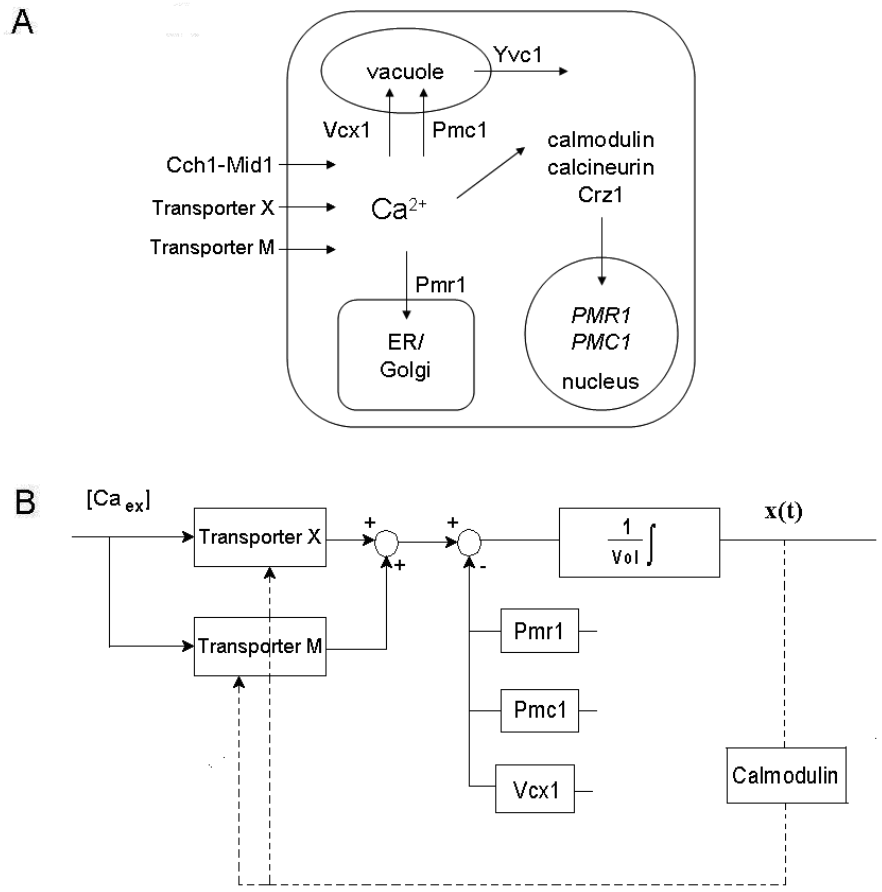

Figure. 3.1. Schematic graph of the system and control block diagram. *Panel A*, A schematic graph of Ca^{2+} homeostasis/signaling system in yeast cells (it is easy to see that this graph is a slightly modified version of Fig. 2.1a). Transporter M is newly detected in this work and is assumed to open under extremely high extracellular Ca^{2+} concentration. *Panel B*, Control block diagram of our model. In *yvc1 cch1* yeast cells, the cytosolic Ca^{2+} influx is through Transporter X and an assumed Transporter M, the cytosolic Ca^{2+} outflux is through Pmc1, Pmr1 and Vcx1. The dashed lines describe the feedback regulations: cytosolic Ca^{2+} concentration is sensed by the calmodulin and Ca^{2+}-bound calmodulin is assumed to inhibit the activity of both transporters M and X.

Here we show that the calcineurin-dependent feedback networks described above have little or no effect on aequorin luminescence traces within the first few minutes of Ca^{2+} shock. Therefore, the initially complex dynamics of cytosolic Ca^{2+} homeostasis must arise through other mechanisms. The observed dynamics are well described by a new mathematical model that omits calcineurin-dependent feedback and instead includes rapid Ca^{2+}-dependent feedback inhibition of Ca^{2+} influx. Though the feedback mechanism and the Ca^{2+} influx transporters all remain to be identified, experimental

evidence suggests that the primary Ca^{2+} influx transporters are competitively inhibited by extracellular Mg^{2+}. Indeed, the impaired growth of yeast cells in high calcium environments was ameliorated by inclusion of Mg^{2+} salts in the medium and the best fitting mathematical model incorporates two Mg^{2+}-sensitive Ca^{2+} influx pathways with different cation affinities. These findings extend a recent report of Ca^{2+} influx pathways in yeast that become (re)activated upon withdrawal of extracellular Mg^{2+} [234] and demonstrate the power of combining experimental and computational methodologies.

3.2 Methods

3.2.1 Experimental Methods

The ability of extracellular Mg^{2+} to prevent toxicity of extracellular Ca^{2+} to yeast was measured as in [50]. Briefly, stationary phase cultures of each yeast strain were diluted 1000-fold into fresh YPD pH 5.5 medium containing varying concentrations of $CaCl_2$ and $MgCl_2$, incubated at 30°C for 24 hr, and then optical density was measured at 650 nm using a 96-well platereader (Molecular Devices). The concentration of $CaCl_2$ causing a 50% inhibition of growth (the IC_{50}) was obtained by fitting the data to the simple sigmoid equation.

Cytosolic free Ca^{2+} concentrations were monitored in populations of yeast cells expressing aequorin essentially as described [150]. Briefly, yeast cells were transformed with plasmid pEVP11 and grown to mid-log phase in synthetic medium lacking leucine to select for plasmid maintenance. Cells were harvested by centrifugation, washed, and resuspended at OD600 = 20 in medium containing 10% ethanol and 25 µg/mL coelenterazine (Molecular Probes, Inc.). After 45 min incubation at room temperature in the dark, cells were washed twice with YPD pH 5.5 medium and shaken at 30°C for an additional 90 min. Aliquots of the cell suspension (450 µL) were pipetted into tubes containing appropriate volumes of 1 M $MgCl_2$, mixed, and placed into a Sirius tube luminometer (Berthold Inc.). Luminescence was recorded at 0.2 sec intervals for 0.5 min prior to and 3.0 min post injection of 2 M $CaCl_2$ (300 µL). Output is plotted as relative luminescence units per second (RLU) over time using similar numbers of cells per sample.

3.2.2 Mathematical Modeling

3.2.2.1 Control Block Diagram

In the control block diagram as shown in Fig. 3.1B, we can see that for yeast cells with fixed volume, we can calculate the concentration of cytosolic Ca^{2+} (i.e., $x(t)$) by taking an integral of the flux rate difference (i.e., the influx rate through Transporter M and Transporter X into the cytosol subtracting the sequestering rates of Pmc1, Pmr1 and Vcx1) divided by the cytosolic volume. Since the slow gene expression feedback pathway through calcineurin has now been shown not to be accounting for the observed response

spikes, there should be some other quick feedback mechanisms the details of which we are currently quite ignorant to. Since calmodulin has been reported to have the ability of directly regulating the opening probability of Ca^{2+} influx pathways [243] , here for simplicity, we just assume that the activity of Transporter M and Transporter X are both directly inhibited by Ca^{2+}-bound calmodulin (see the dashed lines in Fig. 3.1B). If the volume of yeast cells changes due to growth or hypertonic shock etc., then we need to further consider the effects caused by the cellular volume change.

The mathematical modeling for simulating calcium response curves in *yvc1 cch1* yeast cells can now be divided into three parts: feedback modeling, protein modeling (including Transporter M, Transporter X, Pmc1, Pmr1 and Vcx1) and volume evolution modeling.

3.2.2.2 Feedback Modeling

Sensing cytosolic Ca^{2+}: Here we use the same equation as Eq. 2.2 to describe the cytosolic Ca^{2+} sensing process by yeast calmodulin:

$$m'(t) = k_M^+([CaM_{total}] - m(t))x(t)^3 - k_M^- m(t) \tag{3.1}$$

Where $m(t)$ denotes the concentration of Ca^{2+}-bound calmodulin and $m'(t)$ denotes its change rate, k_M^+ denotes the forward rate constant, k_M^- denotes the backward rate constant, $x(t)$ denotes cytosolic calcium ion concentration and $[CaM_{total}]$ denotes the total concentration of calmodulin (including Ca^{2+}-free and Ca^{2+}-bound form).

Once we know the concentration of Ca^{2+}-bound calmodulin, we can use algebraic expressions to model its presumed inhibitory regulation on Transporter M and Transporter X as follows:

$$J_M = J_{MO}/(1 + k_a \times m(t)) \tag{3.2}$$
$$J_X = J_{XO}/(1 + k_b \times m(t)) \tag{3.3}$$

where k_a, k_b denote the feedback control constants. J_M and J_X denote the calcium ion flux through Transporter M and Transporter X respectively. J_{MO} and J_{XO} denote the calcium ion flux through Transporter M and Transporter X in the case of without calmodulin inhibition. Obviously with such simple algebraic expressions the inhibitory relation (i.e., when $m(t)$ rises, the activity of Transporter M and Transporter X will both drop) can be represented.

3.2.2.3 Volume Evolution Modeling (Under Hypertonic Shock)

As we will see later, our aequorin response curves are all obtained under condition of applying hypertonic shocks (e.g., by the sudden injection of 800 mM $CaCl_2$ into the extracellular medium) to the yeast cells. Under such great osmotic perturbation, yeast

cells will quickly shrink due to the existence of water channels in the plasma membrane [79,56,206]. The evolution of the cell volume is governed by the following equation [56]:

$$V'(t) = -A(t)L_p\sigma(\prod_{ex} - RTn_s/(V(t)-b)) \tag{3.4}$$

Where $V(t)$ and $A(t)$ denote the volume and the surface area of yeast cells at time t, respectively, $V'(t)$ denotes the change rate of yeast cell volume, L_p denotes the hydraulic membrane permeability, σ denotes the reflection coefficient, R denotes the ideal gas constant, T denotes the room temperature (294.15 K), n_s denotes the apparent number of osmotically active molecules in the cell, b denotes the non-osmotic volume and $\prod_{ex}$ denotes the osmotic pressure of the external medium which can be calculated as $\prod_{ex} = \prod_0 + 3([Ca_{ex}] + [Mg_{ex}])RT$ where $\prod_0$ denotes the initial osmotic pressure of the external medium, $[Ca_{ex}]$ and $[Mg_{ex}]$ denote extracellular Ca^{2+} concentration and extracellular Mg^{2+} concentration respectively (Please note that we can calculate $A(t) = 4\pi(3V(t)/4/\pi)^{2/3}$ because yeast cells are somewhat spherical).

The initial intracellular osmotic pressure ($\prod_i(0)$) for yeast cells in standard medium is around 0.636 Osm [79], according to Boyle van't Hoff's law, $\prod_i(t) = RT(n_0 + x(t))/(V(t)-b)$ where $x(t)$ denotes cytosolic calcium ion concentration. This means that the initial apparent number of osmotically active molecules n_0 in yeast cell is around 0.636*0.4 mol/l* V_0 = 3.82 *10^{-14}mol (please note that b is 0.4 V_0 and V_0=100μm^3 is the initial volume of the yeast cell [79]). As a common knowledge, $x(t)$ is always <1mM (even under extremely high hypertonic shock) which is small compared with n_0. So we can assume $n_s = n_0 + x(t)$ as a constant.

3.2.2.4 Protein Modeling

Experimental results show that the uptake behavior of the four involved proteins (Transporter X [132], Pmc1 [215], Pmr1 [205] and Vcx1 [159]) conform to the Michaelis-Menten equation, which is a general equation for describing the single site ion uptake behavior of many kinds of transport proteins [5,41]. If we assume that the uptake behavior of Transporter M can also be modeled using this equation and that Mg^{2+} is a competitive inhibitor of this transporter, according to the classical enzyme kinetics theory of competitive inhibition (see Section 1.5.2) [58,178], the uptake rate of Transporter M can be expressed as :

$$J_{MO} = \frac{V_{\max} \times [Ca_{ex}]}{K_m(1 + [Mg_{ex}]/K_{IM}) + [Ca_{ex}]} \tag{3.5}$$

where J_{MO} denotes the uptake rate of Transporter M (without calmodulin inhibition), $[Ca_{ex}]$ and $[Mg_{ex}]$ denote extracellular Ca^{2+} concentration and extracellular Mg^{2+}

concentration respectively, $V_{\max}$ is the maximum uptake rate of Transporter M, K_m is the binding constant and K_{IM} is the inhibition constant. And we can build a similar mathematical model for Transporter X which has been shown to be Mg^{2+}-sensitive [132].

3.2.2.5 A Concise Model

Since now we have built the uptake models for all the five proteins involved in Ca^{2+} transport and models for the relevant feedback regulation, according to the control block diagram (Fig. 3.1B) and by further taking consideration of the effect of cell volume shrinkage, we can derive the main equation of our calcium homeostasis problem as follows [69]:

$$x'(t) = f \times ((J_M + J_X - J_{Pmc1} - J_{Vcx1} - J_{Pmr1}) - x(t)Vol'(t)) / Vol(t) \tag{3.6}$$

Where $x'(t)$ denotes the change rate of cytosolic free Ca^{2+} concentration, J_M, J_X, J_{Pmc1} J_{Vcx1} and J_{Pmr1} denote the calcium ion flux through Transporter M, Transporter X, Pmc1, Vcx1 and Pmr1 respectively, $Vol(t)$ denotes the volume of the cytosol at time t which can be roughly calculated as $10\%V(t)$ and $Vol'(t)$ denotes its change rate, f denotes the calcium buffer effect constant [69]. As stated in page 105 of Ref. 69, "f_i (i.e., f) can be interpreted as the fraction of $[Ca^{2+}]_i^{tot}$ (i.e., total cytosolic calcium) which is free. Typical measured values for f_i are 0.01-0.05." In yeast cells, the calcium buffer effect is especially severe (we believe that >99% of total cytosolic calcium is bound).

We can further write the above main equation in fully detailed mathematical form:

$$x'(t) = f \times \Big(\underbrace{\frac{1}{1+k_a m(t)} \frac{V_m \times [Ca_{ex}]}{K_m(1+[Mg_{ex}]/K_{IM}) + [Ca_{ex}]}}_{TransporterM} + \underbrace{\frac{1}{1+k_b m(t)} \frac{V_x \times [Ca_{ex}]}{K_x(1+[Mg_{ex}]/K_{IX}) + [Ca_{ex}]}}_{TransporterX}$$
$$- \underbrace{\frac{V_1 \times x(t)}{K_1 + x(t)}}_{Pmc1} - \underbrace{\frac{V_2 \times x(t)}{K_2 + x(t)}}_{Pmr1} - \underbrace{\frac{V_3 \times x(t)}{K_3 + x(t)}}_{Vcx1} - V'(t)x(t)) / V(t)\Big) \tag{3.7}$$

where $x(t)$ denotes cytosolic calcium ion concentration, m(t) denotes the concentration of Ca^{2+}-bound calmoculin, K_m, K_x, K_1, K_2 and K_3 are the Michaelis binding constants of Transporter M, Transporter X, Pmc1, Vcx1 and Pmr1 respectively, V_m, V_x, V_1, V_2 and V_3 are the corresponding rate parameters.

Previously published data [132] show that after 2.5 h of incubation, the maximum Ca^{2+} accumulation due to Transporter X is around 390nmol/10^9 cells. We can roughly calculate parameter V_x in the main equation (Eq. 3.7) as follows (for details, please see Eq. 2.18):

$$V_x = V_{\max}/10\% = 2*390nmol/10^9 cells/\int_0^{2.5h} e^{\alpha t}dt/10\% = 3.2*10^{-17} mol\cdot \min^{-1} \quad (3.8)$$

Where α denotes the growth rate constant the value of which is 0.006 $\min^{-1}$[63].

The main equation (Eq. 3.7) together with the calcium sensing equation (Eq. 3.1) and volume evolution equation (Eq. 3.4) constitute a concise mathematical model for simulating response curves in *yvc1 cch1* yeast cells under hypertonic shocks. The whole set of parameters (except the control parameters $[Ca_{ex}]$ and $[Mg_{ex}]$) in our model which will be used in the subsequent simulations are listed in Table 3.1.

Table 3.1: Model parameters for which all results (except Fig. 3.4C) are calculated unless otherwise stated[9].

Parameter	Value	Description
K_m	505.43 mM	the binding constant of Transporter M
K_x	500 μM	the binding constant of Transporter X [132]
K_1	4.3 μM	the binding constant of Pmc1 [215]
K_2	0.1 μM	the binding constant of Pmr1 [205]
K_3	25 μM	the binding constant of Vcx1 [63]
K_{IM}	149.18 mM	the Mg^{2+} inhibition constant of Transporter M
K_{IX}	3.51*10^{-6} μM	the Mg^{2+} inhibition constant of Transporter X
V_m	1.239*10^{-16} mol·$\min^{-1}$	the rate parameter of Transporter M
V_x	3.2*10^{-17} mol·$\min^{-1}$	the rate parameter of Transporter X (Calculated from [132])
V_1	4.459*10^{-17} mol·$\min^{-1}$	the rate parameter of Pmc1
V_2	4.394*10^{-17} mol·$\min^{-1}$	the rate parameter of Pmr1
V_3	1.682*10^{-15} mol·$\min^{-1}$	the rate parameter of Vcx1

[9] Please note that in Table 3.1, thirteen parameters including $K_m, K_{IM}, K_{IX}, V_m, V_1, V_2, V_3, k_a, k_b, k_M^+, k_M^-, L_{\max}$ and f are estimated values by doing optimal fitting to the experimental data for the two transporters model using an hybrid optimization method (see Section 3.2.3: **Parameter Estimation Method).**

k_a	0.0448	the feedback control constant of Transporter M
k_b	4.319	the feedback control constant of Transporter X
k_M^+	3.751 $(\mu M)^{-3}min^{-1}$	the forward rate constant of Eq. 3.1
k_M^-	0.02445 min^{-1}	the backward rate constant of Eq. 3.1
$[CaM_{total}]$	25 μM	the total concentration of calmodulin [183]
$L_{\max}$	$1.9996*10^9$ RLUs	the maximal aequorin luminescence
f	0.007626	the calcium buffer effect constant
L_p	$6*10^{-12} m \cdot s^{-1} \cdot Pa^{-1}$	the hydraulic membrane permeability [56]
σ	0.035	the reflection coefficient
b	0.4 V_0	the non-osmotic volume of yeast cell [79]
n_s	$3.82 *10^{-14}$mol	the apparent number of osmotically active molecules in the cell (calculated from [79])
$\prod_0$	0.24 Osm	the initial osmotic pressure of the external medium [79]
V_0	$100\mu m^3$	the initial volume of the yeast cell [79]

3.2.2.6 Conversion to Aequorin Luminescence Unit (RLUs)

Here we use the following experimentally reported function [7,88] to convert calcium ion concentration from μM to aequorin luminescence unit (i.e., RLU: relative luminescence unit) so that we can make intuitive comparison between our numerical solutions (in μM) with experimentally obtained aequorin response curves (in RLU):

$$y(x) = \left(\frac{1+7x}{1+118+7x}\right)^3 \times L_{\max} \tag{3.9}$$

Where x denotes Ca^{2+} concentration value in unit μM and $L_{\max}$ denotes the maximal aequorin luminescence.

3.2.3 Parameter Estimation Method

The above described two transporters model (Eqs. 3.1, 3.4, 3.7. We name this model as two transporter model because in this model, it is assumed that there are two influx pathways: Transporters M and X) has 25 parameters, 13 of which ($K_m, K_{IM}, K_{IX}, V_m, V_1, V_2, V_3, k_a, k_b, k_M^+, k_M^-, L_{\max}$ and f) are free parameters which need

to be estimated[10]. Here we use a hybrid optimization algorithm to estimate the model parameters by minimizing the difference between the experimental data and the model prediction. The hybrid optimization algorithm consists of a combination of a stochastic evolutionary algorithm [23, 152] for the global search to find a good initial guess followed by a local search performed using Levenberg-Marquardt algorithm to refine the quality of the fit.

To describe a bit more specifically, the stochastic evolutionary algorithm is a stochastic process that modifies an original population of individuals from iteration to iteration with the aim of minimizing an objective function. In this study, we use a modified (μ, λ)-Evolutionary Strategy (ES), based on stochastic fitness ranking [23, 152]. This method is simple and has proven to be more efficient than most other classical evolutionary algorithms for large parameter estimation problems [147, 180, 181]. The local search was performed using the Matlab (The Mathworks, Inc) function "LSQCURVEFIT" which employs Levenberg-Marquardt algorithm to do the curve fitting for non-linear data.

We simultaneously fit the model to both the wild-type data (see Fig. 3.2B) and the mutant data (see Fig. 3.2C) by minimizing the least square error (LSE). As usual, we proportionally weight the wild-type data based on the maximum amplitude of each data set and take mutant data weight to be 1/3 of the wild-type data because the mutant data is less important than the wild-type data. This leads us to minimize the weighted least square error given as:

$$F(\theta) = \sum_{a=1}^{2} \sum_{m=1}^{5} \sum_{n=0}^{n=Tn} w_{a,m,n} (Y_{a,m}^{n} - F(a,m,n))^2 \tag{3.10}$$

where a denotes the type of data (wild-type or mutant). Let $S = \{0, 0.3\text{mM}, 3\text{mM}, 30\text{mM}, 90\text{ mM}\}$, then m denotes the case in which extracellular $MgCl_2$ is the m th element of S. n denotes the time point and Tn denotes the number of data points in the dataset for a single experimental response curve. Thus $Y_{a,m}^{n}$ denotes the concentration for the data type a with extracellular Mg^{2+} = S[m] at time $t = n * td$ where td denotes the time difference between the consecutive data points (in our case, $td = 0.2s$ and $Tn = 300$), $F(a,m,n)$ is the simulated data and $w_{a,m,n}$ is the associated weight.

In addition to fitting the two transporters model to the experimental data, we also performed fitting for the one transporter model. In this case, Transporter X is assumed to be the only influx pathway (i.e., under the condition of $V_m = 0$, Eqs. 3.1, 3.4, 3.7 constitute the one transporter model) and only 9 parameters ($K_{IX}, V_1, V_2, V_3, k_b, k_M^+, k_M^-, L_{\max}$ and f) are free parameters which need to be estimated. Because of the stochastic nature of the optimization strategy used here, lots of fitting

[10] Here we did not include σ because the solution curve of $x(t)$ is extremely insensitive to the value change of this parameter and this will be further discussed in the sixth paragraph of Section 3.4.

were made for both the one transporter and two transporters model[11]. In order to be able to compare both models, the same parameter boundary was given for each parameter and the optimization was run under the same condition (500 iterations of global search and 10000 iterations of local search). The estimated parameters values together with the remaining parameter values for the best fit of two transporters model are shown in Table 3.1. The simulation results of the best fit for two transporters model and for one transporter model are shown in Fig. 3.4A-C.

3.3 Results

3.3.1 Mg^{2+} Blocks Ca^{2+} Toxicity and Ca^{2+} Influx in Yeast

Yeast mutants lacking the vacuolar Ca^{2+} ATPase Pmc1p grow as well as wild-type yeast strains in standard culture media but they grow much poorer than the wild-type when environmental Ca^{2+} is elevated [50], suggesting that elevated cytosolic free Ca^{2+} can be toxic to yeast. However, we noticed that Ca^{2+} toxicity was blocked by a contaminant present in certain batches of agar (data not shown). The contaminant that blocked Ca^{2+} toxicity was traced to Mg^{2+} because (1) the toxicity blocking activity was abolished by addition of the Mg^{2+} chelator EDTA, (2) crude preparations of agar are known to contain millimolar Mg^{2+}, and (3) pure $MgCl_2$ but not NaCl could block Ca^{2+} toxicity in *pmc1* mutants in standard culture media.

To investigate the mechanism of Mg^{2+} suppression of Ca^{2+} toxicity, the concentration of $CaCl_2$ that caused a 50% inhibition of growth (i.e., the IC_{50} for $CaCl_2$) was determined for *pmc1* mutants after 24 hours of growth standard YPD culture medium supplemented with 0 to 32 mM $MgCl_2$. Remarkably, for *pmc1* knockout mutants the IC_{50} for $CaCl_2$ increased with increasing $MgCl_2$ up to ~8 mM after which the effectiveness of $MgCl_2$ began to decrease (Fig. 3.2A, filled circles). Double mutants lacking both Pmc1 and the vacuolar Ca^{2+}/H^+ exchanger Vcx1 behaved similarly except the IC_{50} values were shifted downward by ~1.6 fold (Fig. 3.2A, open circles). The sole remaining Ca^{2+} transporter Pmr1, a Ca^{2+}/Mn^{2+} ATPase of the Golgi complex, is essential for growth of *pmc1 vcx1* double mutants and is strongly up-regulated by calcineurin [51]. A *pmc1 vcx1 cnb1* triple mutant that also lacks calcineurin exhibited ~2.3 fold lower tolerance to $CaCl_2$ than the *pmc1 vcx1* double mutant and $MgCl_2$ suppressed $CaCl_2$ toxicity over a similar range of concentrations (Fig. 3.2A, filled triangles). A *vcx1 cnb1* double mutant in which Pmc1 and Pmr1 are expressed only at basal levels exhibited ~6.6-fold increase of IC_{50} for $CaCl_2$ as expected and also exhibited $MgCl_2$ suppression of $CaCl_2$ toxicity (Fig. 3.2A, open triangles). These findings demonstrate that $MgCl_2$ suppresses $CaCl_2$ toxicity independent of all known Ca^{2+} transporters, which is consistent with the possibility that Mg^{2+} competitively inhibits one or more Ca^{2+} influx pathways.

[11] Simulation results show that the weighted least square error defined in Eq. 3.10 is quite sensitive to the value of K_{IX}, the reason of which will be further discussed in the second paragraph of Section 3.4. In each optimal fitting, we does not get the same optimal solution. So we choose the best solution with the lowest weighted least square error as defined in Eq. 3.10 after having done a lot of fittings.

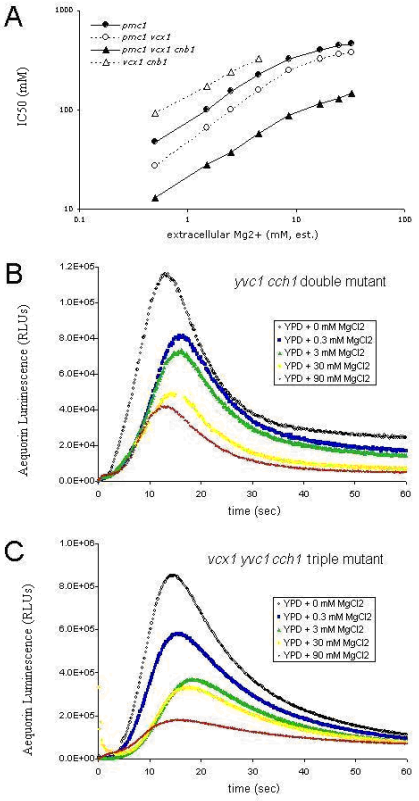

Figure. 3.2. Experimental results. *Panel A*, the concentrations of $CaCl_2$ that caused a 50% inhibition of growth (i.e., the IC_{50} for $CaCl_2$) were shown for *pmc1* (filled circles), *pmc1 vcx1* (open circles), *pmc1 vcx1 cnb1* (filled triangles) and *vcx1 cnb1* (open triangles) mutants after 24 hours of growth standard YPD culture medium supplemented with 0 to 32 mM $MgCl_2$. *Panel B*, A *yvc1 cch1* double mutant expressing apo-aequorin from a plasmid was incubated with coelenterazine co-factor to reconstitute aequorin in situ. The cells bearing reconstituted aequorin were returned to growth medium for an additional 90 minutes, divided into equal aliquots, treated with varying amounts (0, 0.3, 3, 30, 90mM) of $MgCl_2$, placed into a tube luminometer, and monitored for luminescence before and after injection of 800 mM $CaCl_2$. *Panel C,* the corresponding aequorin luminescence curves for *vcx1 yvc1 cch1* mutant.

Two Ca^{2+} channels have been characterized in yeast, the vacuolar Ca^{2+} release channel Yvc1 and the plasma membrane Ca^{2+} influx channel Cch1-Mid1. The *yvc1 cch1 pmc1 vcx1* quadruple mutant exhibited similar levels of $MgCl_2$ suppression of $CaCl_2$ toxicity as the *pmc1 vcx1* double mutants (data not shown), suggesting that Mg^{2+} blocks some other Ca^{2+} influx pathways. To test this possibility directly, cytosolic free Ca^{2+} concentrations were monitored directly after a sudden increase in extracellular $CaCl_2$ by following luminescence of the Ca^{2+}-sensitive photoprotein aequorin. The *yvc1 cch1* double mutant expressing apo-aequorin from a plasmid was incubated with coelenterazine co-factor to reconstitute aequorin in situ. The cells bearing reconstituted aequorin were returned to growth medium for an additional 90 minutes, divided into equal aliquots, treated with

varying amounts of $MgCl_2$, placed into a tube luminometer, and monitored for luminescence before and after injection of 800 mM $CaCl_2$. In the absence of added $MgCl_2$, aequorin luminescence rose quickly after $CaCl_2$ injection, peaked after ~13.3 sec, and declined to a level that was well above the starting level (Fig. 3.2B). Increasing concentrations of $MgCl_2$ progressively lowered the rates of luminescence rise, the maximum achievable luminescence, and the new baseline levels following decline (Fig. 3.2B). Remarkably, the loss of Vcx1 resulted in a dramatic increase in the rate and peak height of aequorin luminescence (Fig. 3.2C). Additionally, the loss of Vcx1 resulted in ~60% slower rate of luminescence decline after the peak regardless of $MgCl_2$ concentration. Though calcineurin inhibits Vcx1 function in long-term growth assays [51], the activity of Vcx1 in these short-term luminescence experiments was not detectably affected by addition of the calcineurin inhibitor FK506 (data not shown). The further loss of Pmc1 also had little effect on aequorin responses (data not shown). These findings identify Vcx1 as the major Ca^{2+}-sequestering transporter in short-term responses to high Ca2+ environments and confirm the hypothesis that Mg^{2+} interferes with one or more novel Ca^{2+} influx pathways. A similar hypothesis was proposed recently to explain the increased Ca^{2+} influx and elevated cytosolic Ca^{2+} concentration observed in yeast upon Mg^{2+} sudden withdrawal [234]. The proteins responsible for Mg^{2+}-sensitive Ca^{2+} influx have not been identified but the Alr, Alr2, and Mnr2 proteins have been identified as hetero-oligomeric proteins required for Mg^{2+} uptake that also promote sensitivity to high environmental Ca^{2+} [134].

3.3.2 Computational Modeling of Ca^{2+} Influx and Sequestration

The multiphasic nature and calcineurin-independence of the aequorin luminescence curves suggested complex dynamics of the novel Ca^{2+} influx pathway(s) as opposed to calcineurin feedback pathways modeled previously (see Chapter 2). To understand these dynamics, a mathematical model was constructed in which the Ca^{2+} transporters Pmr1, Pmc1, and Vcx1 were assumed to function without calcineurin feedback *in vivo* according to standard Michaelis-Menten kinetics. The optimal fitting to the experimental data using a hybrid optimization algorithm (see Section 3.2.3: **Parameter Estimation Method**) shows that simulations assuming two Mg^{2+}-sensitive Ca^{2+} influx transporters (termed transporters M and X) each with distinct properties (as discussed below in more detail) can closely fit the experimental data (see Fig. 3.4A-B and compare them with Fig. 3.2B-C) whereas simulations using just one Mg^{2+}-sensitive Ca^{2+} influx transporter poorly fit the experimental data (see Fig. 3.4C and compare it with Fig. 3.2B).

3.3.2.1 Steady-State Properties

The model for *yvc1 cch1* mutant under hypertonic shock consists of three equations (Eqs. 3.1, 3.4, 3.7, please see Section 3.2.2: **Mathematical modeling**) with three unknowns: $x(t)$, $m(t)$ and $V(t)$. By performing steady state analysis of our model with fixed parameter $[Ca_{ex}]$=800mM, we can first depict the steady state value of $x(t)$ as a function of parameter $[Mg_{ex}]$ as shown in Fig. 3.3A. In general, the resting level of $x(t)$ decreases

almost linearly as $[Mg_{ex}]$ increases. Only in the case of very low $[Mg_{ex}]$ (≤1μM), the curve shows a strange bending.

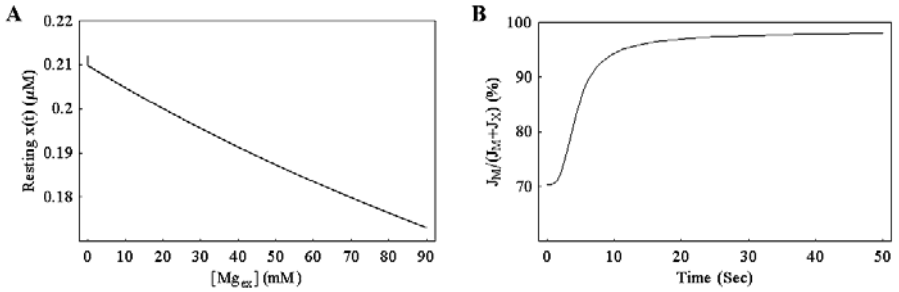

Figure. 3.3. Steady state analysis and flux analysis of the system. *Panel A,* the steady state value of $x(t)$ as a function of parameter $[Mg_{ex}]$ for simulated *yvc1 cch1* mutant in extracellular medium with high calcium concentration (parameter $[Ca_{ex}]$ = 800mM). The simulated cytosolic calcium level of our model *yvc1 cch1* mutant rests within 0.173-0.212μM (regardless of the initial conditions) as the media Mg^{2+} level (parameter $[Mg_{ex}]$) ranges from 0mM to 90mM. *Panel B,* the simulated flux proportion of Transporter M in the total cytosolic Ca^{2+} influx as a function of t for *yvc1 cch1* mutant under hypertonic shock (at $t = 0$, parameter $[Ca_{ex}]$ suddenly increases from 0mM to 800mM and at the same time parameter $[Mg_{ex}]$ suddenly increases from 0 mM to various concentrations. Please note that the curve shown in this graph is for $[Mg_{ex}] = 0mM$. For all the other cases (i.e., $[Mg_{ex}]$ =0.3 mM, 3 mM, 30 mM, 90 mM), the simulated curves coincide with the top frameline (i.e., $J_M/(J_M + J_X) = 100\%$).

3.3.2.2 Transients and Mutant Behavior

By setting reasonable initial conditions ($x(0) = 100nM$, $m(0) = 0M$ and $V(0) = 100\mu M^3$) and then solving the three equations (Eqs. 3.1, 3.4, 3.7, using the parameters listed in Table 3.1) numerically, we can depict the $x(t)$ curves for parameter $[Mg_{ex}]$ suddenly increasing from 0 mM to various concentrations (0 mM, 0.3 mM, 3 mM, 30 mM, 90 mM) at $t = 0$ as shown in Fig. 3.4A (please note that at the same time, parameter $[Ca_{ex}]$ suddenly increases from 0mM to 800mM in these simulations). In general, the simulated $x(t)$ rises due to the hypertonic shock, forms a peak and then declines to a resting value; for higher value of parameter $[Mg_{ex}]$, the peak value of the curve is lower and appears later. For example, by observing the top black curve for parameter $[Mg_{ex}]$=0mM, we can see that due to the hypertonic shock, the simulated $x(t)$ quickly rises (in around 9 seconds) from an initial value of 5,700RLUs (~100nM) to a high peak of around 116,600RLUs (~0.54μM) , then gradually decreases to a value of 46,110RLUs (~0.35μM) when $t = 1\min$. Further investigation shows that it will further decreases to steady state value of 17,500RLUs (~0.21μM). By observing the blue curve for parameter $[Mg_{ex}]$ rising

from 0mM to 0.3mM, we can see that the simulated cytosolic $x(t)$ rises slower than the black curve and its peak value (around 85,200RLUs(~0.47μM)) which appears when $t = 14$ sec is much lower than that of the black curve. However, the green curve for parameter $[Mg_{ex}]$ rising from 0mM to 3mM seems just a little bit lower and slower than the blue curve.

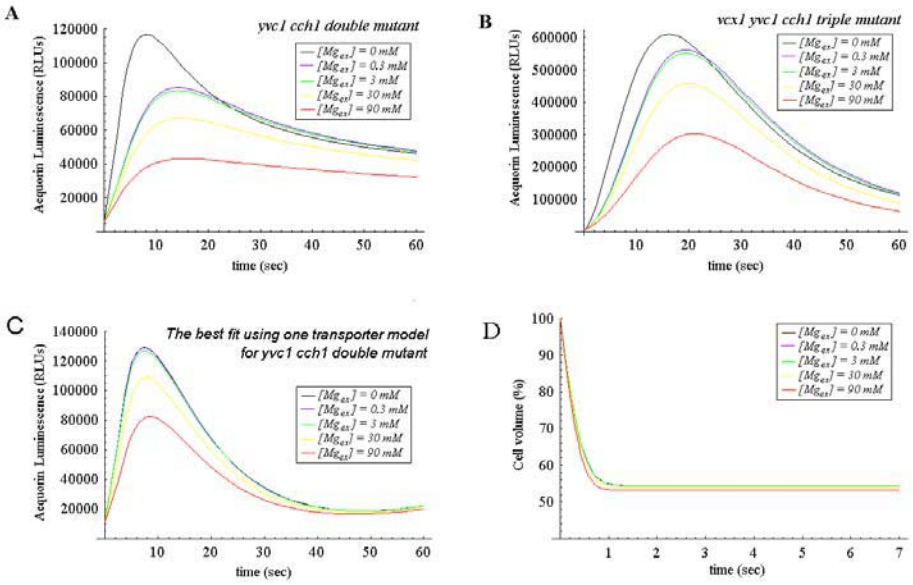

Figure. 3.4. Simulated response curves and volume evolution curves. *Panel A*, the simulated response curves of the best fit using two transporters model for *yvc1 cch1* mutant. The black, blue, green, yellow and red curves depict the simulated $x(t)$ curves for parameter $[Mg_{ex}]$ suddenly increasing from 0 mM to various concentrations (0 mM, 0.3 mM, 3 mM, 30 mM, 90 mM) at $t = 0$ respectively (please note that at the same time $t = 0$ parameter $[Ca_{ex}]$ suddenly increases from 0mM to 800mM in these simulations). *Panel B*, the corresponding simulated response curves using two transporters model for *vcx1 yvc1 cch1* mutant. *Panel C*, the simulated response curves of the best fit using one Mg^{2+}-sensitive transporter model (i.e., in this case we assume that Transporter X is the sole influx pathway) for *yvc1 cch1* mutant. The black, blue, green, yellow and red curves depict the simulated $x(t)$ curves for parameter $[Mg_{ex}]$ suddenly increasing from 0 mM to various concentrations (0 mM, 0.3 mM, 3 mM, 30 mM, 90 mM) at $t = 0$ respectively (please note that at the same time $t = 0$ parameter $[Ca_{ex}]$ suddenly increases from 0mM to 800mM in these simulations). *Panel D*, the simulated volume evolution curves using the two transporters model for *yvc1 cch1* mutant under hypertonic shock (step increase of $[Ca_{ex}]$ from 0mM to 800mM with simultaneous step increase of $[Mg_{ex}]$ to various concentrations). Please note that the black and blue curves coincide with the green curve in this graph.

In Fig. 3.4B, we depict the simulated $x(t)$ curves for *vcx1 yvc1 cch1* triple mutant under hypertonic shock (step increase of $[Ca_{ex}]$ from 0mM to 800mM with simultaneous step increase of $[Mg_{ex}]$ to various concentrations at $t = 0$, please note that V_3 is set to be 0 in these simulations, for the rest parameters please see Table 3.1). By comparison of these

curves with their corresponding curves for simulated *yvc1 cch1* double mutant in Fig. 3.4A, the peak values of these simulated response curves seem much higher. For example, the peak value of the top black curve for $[Mg_{ex}]$=0mM in Fig. 3.4B is around 609,000RLUs (~1.07μM) which is certainly much higher than the peak value 116,600RLUs (~0.54μM) of its corresponding black curve in Fig. 3.4A.

In Fig. 3.4C, the simulated $x(t)$ curves of the best fit using one Mg^{2+}-sensitive transporter model (i.e., Transporter X is assumed to be the only influx pathway) for *yvc1 cch1* mutant under hypertonic shock (step increase of $[Ca_{ex}]$ from 0mM to 800mM with simultaneous step increase of $[Mg_{ex}]$ from 0mM to various concentrations at $t = 0$) are shown. In this figure, the top two curves (i.e., the black curve and the blue curve) coincide with each other. The peak values of the blue, green, yellow, red curves are 129,000RLUs (~0.413μM), 127,000RLUs (~0.41μM), 109,000RLUs (~0.382μM), 82,340RLUs (~0.334μM), respectively. The peaks of both blue and green curves appear when $t = 7.5\,\text{sec}$ whereas the peaks of the yellow and red curves appear at $t = 7.9\,\text{sec}$ and $t = 8.6\,\text{sec}$, respectively.

3.3.2.3 Flux Analysis and Cell Volume Evolution

To discriminate the different influx contributions from two Ca^{2+} influx pathways, in Fig. 3.3B we depict the simulated flux proportion of Transporter M in the total cytosolic Ca^{2+} influx as a function of t for *yvc1 cch1* mutant under hypertonic shock (step increase of $[Ca_{ex}]$ from 0mM to 800mM with simultaneous step increase of $[Mg_{ex}]$ from 0mM to various concentrations at $t = 0$). By observing the black curve for $[Mg_{ex}]$=0mM, we can see that at the beginning, 70.4% of the cytosolic Ca^{2+} influx is contributed by Transporter M and this proportion quickly rises to 98%. The other curves seem to coincide and are flat with a constant value of 100%.

In Fig. 3.4D, the simulated volume evolution curves using to transporters model for *yvc1 cch1* mutant under hypertonic shock (step increase of $[Ca_{ex}]$ from 0mM to 800mM with simultaneous step increase of $[Mg_{ex}]$ from 0mM to various concentrations at $t = 0$) are shown. As we can see in this figure, in general, the cell volume quickly decreases (in about 1 second) to a steady state value of 53-55% percent of the initial volume and the difference among different color curves are quite subtle.

3.3.2.4 Extracellular Mg^{2+} Depletion and Ca^{2+} Challenge

To check the behavior of cytosolic Ca^{2+} level (i.e., $x(t)$) of our model *yvc1 cch1* mutant cell upon extracellular Mg^{2+} depletion, in Fig. 3.5A we depict the simulated $x(t)$ response curve for parameter $[Mg_{ex}]$ suddenly decreasing from 1 mM to 0 mM at $t = 0$ and being reset to 1mM after 90 seconds (parameter $[Ca_{ex}] = 150mM$ in this simulation). From this figure, we can see that when $t = 0$, the simulated cytosolic Ca^{2+} level rises quickly (in 15 seconds) from its original resting level of 0.081μM to a value of 0.099 μM,

almost keeps at that value and recovers quickly to its original resting level of 0.081μM when $t = 1.5\,\text{min}$.

To further check the behavior of cytosolic Ca^{2+} level of our model *yvc1 cch1* mutant cell upon extracellular Ca^{2+} challenge, in Fig. 3.5B we depict the simulated $x(t)$ response curve for parameter $[Ca_{ex}]$ suddenly increasing from 150 mM to 200 mM at $t = 0$ and being reset to 150mM after 90 seconds (parameter $[Mg_{ex}] = 0mM$ in this simulation). From this figure, we can see that the simulated cytosolic Ca^{2+} level rises quickly (in 15 seconds) from its original resting level of 0.091μM to a value of 0.125μM and decreases very gradually to a value of 0.123μM (at $t = 1.5\,\text{min}$), then it decreases quickly to its original resting value.

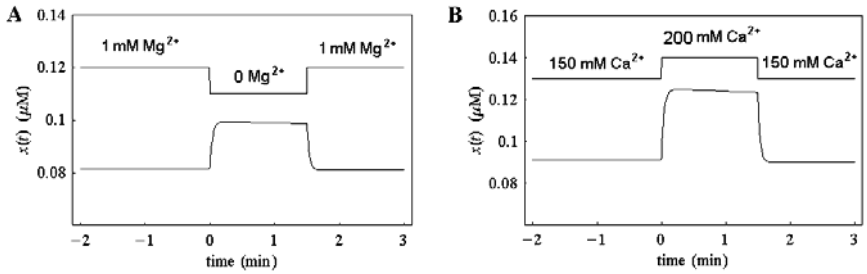

Figure. 3.5. Simulated cytosolic Ca^{2+} level (i.e., $x(t)$) for *yvc1 cch1* mutant increases upon extracellular Mg^{2+} depletion or extracellular Ca^{2+} challenge. *Panel A*, the simulated $x(t)$ response curve (the bottom curve) for parameter $[Mg_{ex}]$ (the top curve) suddenly decreasing from 1 mM to 0 mM at $t = 0$ and being reset to 1mM after 90 seconds (please note that in this simulation, parameter $[Ca_{ex}] = 150mM$). *Panel B*, the simulated $x(t)$ response curve (the bottom curve) for parameter $[Ca_{ex}]$ (the top curve) suddenly increasing from 150 mM to 200 mM at $t = 0$ and being reset to 150mM after 90 seconds (please note that in this simulation, parameter $[Mg_{ex}] = 0mM$). The basal level of $[Ca_{ex}]$ in these two simulations is set to be 150mM instead of 2mM as in Wisenberger's paper [234] because our model is only valid for hypertonic shock (extracellular Ca^{2+} >132mM).

3.4 Discussion

We present experimental data that are consistent with the existence of Mg^{2+}-sensitive Ca^{2+} influx pathways in yeast. Increasing concentrations of extracellular Mg^{2+} increased the concentration of extracellular Ca^{2+} necessary for inhibition of yeast cell growth over a 24 hr period. By extrapolation of log-transformed plots of Mg^{2+} concentration versus IC_{50}, we estimate that standard YPD medium effectively contains 0.5 mM Mg^{2+}, in good agreement with the assayed value of 0.7 mM [2]. Increasing concentrations of extracellular Mg^{2+} also inhibited Ca^{2+} influx as judged by decreasing rates of aequorin luminescence following a sudden increase of extracellular Ca^{2+}. While this work was in

progress, a complementary study also showed that sudden withdrawal of all extracellular Mg^{2+} from synthetic growth medium caused a rapid and reversible influx of Ca^{2+} into yeast cells [234]. An earlier study of $^{45}Ca^{2+}$ influx demonstrated Mg^{2+} inhibition of a constitutive Ca^{2+} influx pathway [132]. Finally, overexpression of the yeast Alr1 or Alr2 Mg^{2+} transporters – homologs of the bacterial CorA Mg^{2+} transporters – resulted in increased sensitivity to high environmental Ca^{2+} [134]. All these results are consistent with a model where Mg^{2+} competitively inhibits one or more Ca^{2+} influx pathways.

As just mentioned, previously published data demonstrate the existence of a constitutive Mg^{2+}-sensitive Ca^{2+} influx pathway, which we called Transporter X [132]. From Fig. 3.2B, we can see that a subtle difference of extracellular Mg^{2+} concentration results in the great difference between the profiles of the black (for $[Mg_{ex}] = 0$) and blue curve (for $[Mg_{ex}] = 0.3mM$). In the case of one transporter model, this can only happen when Transporter X has a very small inhibition constant K_{IX} so that a subtle increase of extracellular Mg^{2+} concentration will have great inhibitory effect on the calcium influx (see Eq. 3.7, please note that $V_m = 0$ for one transporter model. The only influx is through Transporter X which is expressed as $\frac{1}{1+k_b m(t)} \frac{V_x \times [Ca_{ex}]}{K_x(1+[Mg_{ex}]/K_{IX})+[Ca_{ex}]}$. Given fixed V_x, K_x and $[Ca_{ex}]$, smaller K_{IX} can make this influx term more sensitive to the change of $[Mg_{ex}]$). However, a very small K_{IX} will lead to even greater inhibitory effect when $[Mg_{ex}] = 3mM$ or higher concentration. Thus for one transporter model, it either can not reproduce the great difference between the profiles of the black and the blue experimental curves in Fig. 3.2B or can not reproduce the relatively subtle difference between the profiles of the blue and green curves in Fig. 3.2B. However, it is possible for two transporters model to reproduce both differences when in addition to Transporter X with an extremely low K_{IX} which functions only in the case of extremely low extracellular Mg^{2+}, there is another transporter with a high magnesium inhibition constant whose influx is much less sensitive to the change of extracellular Mg^{2+} than that of Transporter X.

As shown in Fig. 3.4C, simulations using just one Mg^{2+}-sensitive Ca^{2+} influx transporter poorly fit the experimental data because the best fit of one Mg^{2+}-sensitive transporter model (see Fig. 3.4C) using hybrid optimization algorithm can not reproduce the great difference between the black and blue experimental curves shown in Fig. 3.2B whereas simulations assuming two Mg^{2+}-sensitive Ca^{2+} influx transporters (termed transporters X and M with very distinct inhibition constants: $K_{IX} = 3.51*10^{-6}$ μM and K_{IM} =149.18 mM) can closely fit the experimental data (see Fig. 3.4A and Fig. 3.4B). All these results confirm the theoretical analysis in the previous paragraph and our simulation results strongly suggest the existence of a new transporter named Channel M on the *yvc1 cch1* mutant. As shown in Fig. 3.3B, for $[Mg_{ex}]$=0 (see the black curve in Fig. 3.3B), both transporters M and X make considerable contribution to the total Ca^{2+} influx whereas for

relatively high $[Mg_{ex}]$ (see Fig. 3.3B) the flux contribution of Transporter X becomes negligible. The strange bending shown in Fig. 3.3A appears because of the opening of Transporter X in the case of extremely low $[Mg_{ex}]$.

A mathematical model of Transporter M and other components of the system was constructed here. By comparison of simulated response curves in Fig. 3.4A with corresponding experimental curve in Fig. 3.2B for *yvc1 cch1* mutant, we can see that the numerical simulations of our model do can quantitatively reproduce the main characteristics of the experimental results such as low levels of extracellular Mg^{2+} can slow Ca^{2+} influx and diminish cytosolic free Ca^{2+} elevation. The model assumed that Transporter M has very low affinity for Ca^{2+} (K_m = 505.43 mM), competitive inhibition by extracellular Mg^{2+} (K_{IM} = 149.18 mM), and rapid feedback inhibition by intracellular Ca^{2+}. The mechanism of feedback was found to be independent of calcineurin but otherwise its components remain wholly unknown. The relatively low affinity for Ca^{2+} relative to Mg^{2+} also suggests that Transporter M may function primarily as a Mg^{2+} transporter in physiological conditions. If so, the cellular response to high extracellular Ca^{2+} may include Mg^{2+} starvation in addition to Ca^{2+} influx, as suggested recently [234]. It is very likely that both transporters M and X are homo/hetero-oligomers of Alr1, Alr2 and Mnr2 - uniporters primarily involved in Mg^{2+} uptake (Please note that uniporter is an inetgral membrane protein that is involved in facilitated diffusion whose uptake behavior can be well described with Michaelis-Menton kinetics [5]). A more realistic understanding of Transporter M and Transporter X should be possible after their genes and regulators are identified and characterized.

The computer simulations (see Fig. 3.4A and Fig. 3.4B) also reproduced the experimentally determined effects of the vacuolar H^+/Ca^{2+} exchanger Vcx1 on cytosolic free Ca^{2+} dynamics. The presence or absence of calcineurin inhibitor had no effect on the aequorin traces in the presence or absence of Vcx1 (data not shown), suggesting no significant inhibition of Vcx1 by calcineurin within three minutes following Ca^{2+} shock. In long-term growth experiments, calcineurin appears to strongly inhibit Vcx1 function in addition to strongly inducing Pmc1 function [51]. Perhaps these effects of calcineurin can be observed in aequorin experiments performed over longer time scales and used to computationally model the long-term effects of Ca^{2+} on yeast growth (Fig. 3.2A).

From Fig. 3.4d, we can see that the shrinkage of our simulated *yvc1 cch1* model cell is quickly accomplished (in less than 1 second). More simulations show that the volume shrinkage rate of our model cell is mainly determined by the reflection coefficient σ, the value of which used here (i.e., 0.035) is actually a value for sorbitol obtained by fitting the experimental curve [56]. Although the reflection coefficient σ for the current solute is not exactly known, further investigations show that the value of σ (in the investigations, we let this value range from 1000 to 0.001) seems to have insignificant influence on our main simulation results shown in Fig. 3.3 and Fig. 3.4A-C.

Wisenberger *et al.* reported in their experimental paper [234] that removal of Mg^{2+} in extracellular medium (with the presence of extracellular Ca^{2+}) resulted in an immediate

increase in free cytoplasmic Ca^{2+} and this signal was reversible. As we can see from Fig. 3.5A, the sudden step decrease of $[Mg_{ex}]$ from 1mM to 0mM at $t = 0$ incurs an immediate quick rise of simulated cytosolic Ca^{2+} level (i.e., $x(t)$) and after parameter $[Mg_{ex}]$ is reset to 1mM at $t = 1.5\,\text{min}$, simulated cytosolic Ca^{2+} drops and recovers to its original resting level. Moreover, by comparison of two simulated response curves shown in Fig. 3.5A and Fig. 3.5B, we can see that the manner of the behavior of the simulated cytosolic Ca^{2+} level under Mg^{2+} depletion is quite similar to that under Ca^{2+} challenge. All these simulation results show that our model can reproduce (although roughly) the relevant experimental results reported by Wisenberger *et al* [234].

Finally there are still two issues worthy of discussion here. The first issue is about the reversibility of Ca^{2+} sequestration through Vcx1 and Pmc1. Intuitively there should exist a Ca^{2+} efflux from the vacuole into the cytosol. However, this is not the case for yeast cells. Dunn *et al.* (1994) ever measured the rate of Ca^{2+} efflux from yeast vacuoles both *in vitro* and *in vivo* [63]. Their experiments indicated that *in vivo* vacuolar Ca^{2+} efflux is very low (essentially zero). We think that it is more appropriate to use standard Michaelis-Menten kinetics (as we did here) rather than reversible Michaelis-Menten kinetics to describe the uptake behavior of Vcx1 and Pmc1 because the later kinetics will introduce an unreal vacuolar Ca^{2+} efflux. The second issue is about the validity of using Michaelis-Menten kinetics for modeling the uptake behavior of the transporters M and X. It is well-known that Michaelis-Menten kinetics assumes a rapid equilibrium between the enzyme and substrate to form an intermediate complex [58]. So we need to check if the uptake of Ca^{2+} and Mg^{2+} through the transporters is fast enough that it could be considered as steady-state at all times. Ion channels enable rapid ($\sim 10^7$ ion s^{-1}) movement of selected ions through pores in biological membranes [19]. Ca^{2+} channel can recognize its substrate and let it permeate within 10-100ns [144]. Carriers (i.e., transporters) are characterized by turnover numbers that are typically 1,000-fold lower than ion channels [117]. This means the average time needed for a Ca^{2+} to pass through the plasma membrane via the help of an ion transporter is within 10-100μs, which is several order smaller than the time frame (in seconds) of the Ca^{2+} peaks shown in Fig. 3.2B and Fig. 3.2C. Moreover, Michaelis-Menten kinetics has been used in a mathematical model for describing the iron uptake behavior of plasma membrane iron transporter in the iron homeostasis system of *E. coli* (see the first term in Eq.1 in Ref. 191). So here we think that it is appropriate to use Michaelis-Menten kinetics for modeling the uptake behavior of the transporters M and X.

As mentioned before, the mathematical model presented here is only valid for a short lapse (about three minutes) following the hypertonic Ca^{2+} shock. This model needs to be modified for low extracellular Ca^{2+} (<132mM) because Eq. 3.4 is only valid for hypertonic shock and it does not include factors such as turgor pressure which will arise in the case of low extracellular Ca^{2+}. Moreover, for simplicity, this model assumes direct inhibition of Ca^{2+}-bound calmodulin on both two transporters M and X, which is not backed by any experimental data. In the real cells, the relevant feedback regulation pathways may be more complicated. And the relative coarseness of the model accounts for the differences (e.g., the noticeable bias in the downward phase of the peak) shown by the comparison of Fig. 3.2B with Fig. 3.4A (also by comparison of Fig. 3.2C with Fig.

3.4B). On the other hand, the novelty of the present work lies in that by combining computational and experimental methodology, we detect the existence of a new Mg^{2+}-sensitive Ca^{2+} transporter named as Transporter M on the yeast plasma membrane of *yvc1 cch1* mutant cell working together with previously found Transporter X under hypertonic Ca^{2+} shock. The eventual accomplishment of a complete and accurate mathematical model of dynamic Ca^{2+} signaling networks in yeast will facilitate similar endeavors in all cell types and organisms, but doing so still requires additional mechanistic insights obtained from the fusion of experimental data and mathematical models.

In this chapter, we have revised and extended the first preliminary model for yeast calcium homeostasis (see Chapter 2) and developed a new mathematical model that omitted calcineurin-dependent feedback and instead included rapid Ca^{2+}-dependent feedback inhibition of Ca^{2+} influx pathways to simulate complex cytosolic free Ca^{2+} dynamics of *yvc1 cch1* yeast cells under hypertonic shock. The validity of the model was confirmed by its ability of reproducing the experimental data (including the experimentally determined effects of Vcx1 on cytosolic free Ca^{2+} dynamics) and simulating the effects of extracellular Mg^{2+} removal. Both models presented in Chapter 2 and Chapter 3 consist of several nonlinear ODEs which seem relatively simple. In Chapter 4, we will describe a much more complicated model for describing calcineurin-dependent calcium signaling network in cardiac myocytes of mice.